THE ASTROPHYSICAL JOURNAL, 624:L5–L8, 2005 May 1

CONSTRAINTS ON $z \approx 10$ GALAXIES FROM THE DEEPEST *HUBBLE SPACE TELESCOPE* NICMOS FIELDS[1]

R. J. BOUWENS,[2] G. D. ILLINGWORTH,[2] R. I. THOMPSON,[3] AND M. FRANX[4]

Received 2005 January 9; accepted 2005 March 15; published 2005 April 4

ABSTRACT

We use all available fields with deep NICMOS imaging to search for J_{110}-dropouts ($H_{160,AB} \lesssim 28$) at $z \approx 10$. Our primary data set for this search is the two $J_{110} + H_{160}$ NICMOS fields taken in parallel with the Advanced Camera for Surveys (ACS) Hubble Ultra Deep Field (UDF). The 5 σ limiting magnitudes were ~28.6 in J_{110} and ~28.5 in H_{160} (0.″6 apertures). Several shallower fields were also used: $J_{110} + H_{160}$ NICMOS frames available over the Hubble Deep Field (HDF) North, the HDF-South NICMOS parallel, and the ACS UDF (with 5 σ limiting magnitudes in J_{110} and H_{160} ranging from 27.0 to 28.2). The primary selection criterion was $(J_{110}-H_{160})_{AB} > 1.8$. Eleven such sources were found in all search fields using this criterion. Eight of these are clearly ruled out as credible $z \approx 10$ sources, either as a result of detections (>2 σ) blueward of J_{110} or their colors redward of the break ($H_{160}-K \sim 1.5$) (redder than $\gtrsim$98% of lower redshift dropouts). The nature of the three remaining sources could not be determined from the data. This number appears consistent with the expected contamination from low-redshift interlopers. Analysis of the stacked images for the three candidates also suggests some contamination. Regardless of their true redshifts, the actual number of $z \approx 10$ sources must be three or fewer. To assess the significance of these results, two lower redshift samples (a $z \sim 3.8$ *B*-dropout and $z \sim 6$ *i*-dropout sample) were projected to $z \sim 7$–13 using a $(1 + z)^{-1}$ size scaling (for fixed luminosity). They were added to the image frames and the selection was repeated, giving 15.6 and 4.8 J_{110}-dropouts, respectively. This suggests that to the limit of this probe ($\approx 0.3L^*_{z=3}$), there has been evolution from $z \sim 3.8$ and possibly from $z \sim 6$. This is consistent with the strong evolution already noted at $z \sim 6$ and $z \sim 7.5$ relative to $z \sim 3$–4. Even assuming that three sources from this probe are at $z \approx 10$, the rest-frame continuum UV (~1500 Å) luminosity density at $z \sim 10$ (integrated down to $0.3L^*_{z=3}$) is just $0.19^{+0.13}_{-0.09}$ times that at $z \sim 3.8$ (or $0.19^{+0.15}_{-0.10}$ times, including the small effect from cosmic variance). However, if none of our sources are at $z \approx 10$, this ratio has a 1 σ upper limit of 0.07.

Subject headings: galaxies: evolution — galaxies: high-redshift

Online material: machine-readable table

1. INTRODUCTION

The detection of galaxies at the highest redshifts ($z \gtrsim 7$) continues to be a difficult endeavor. Because of the redshifting of UV light into the infrared and the well-known limitations of current IR instruments, searches for these objects require almost prohibitive amounts of telescope time. Nevertheless, small amounts of deep IR data do exist, and they can be used to set constraints on very high redshift galaxies. One notable example is the z_{850}-dropout sample compiled in Bouwens et al. (2004c), which, although limited by small numbers (five objects) and field-to-field variations, provided a first detection of galaxies at redshifts beyond $z \sim 7$. In this Letter, we look at the prevalence of galaxies at $z \sim 8$–12 by applying the dropout technique to the wide variety of deep F110W- and F160W-band (hereafter J_{110} and H_{160}, respectively) fields that have been imaged with the Near Infrared Camera and Multi-Object Spectrometer (NICMOS). Our principal data set in this study is the two deep NICMOS parallels taken with the Ultra Deep Field (UDF; each has ~160 orbits of data), but we complement this field with a variety of shallower fields possessing similar $J_{110} + H_{160}$ imaging. These fields include the Hubble Deep Field–North (HDF-N) Thompson field (Thompson et al. 1999), the HDF-N Dickinson field (Dickinson 1999), the deep HDF-South parallel NICMOS field (Williams et al. 2000), and the NICMOS footprint on the UDF itself (Thompson et al. 2005). Galaxies in the range $z \sim 8$–12 are currently of great interest due to indications that reionization of the universe may have started as soon as $z \sim 17 \pm 5$ (Kogut et al. 2003) and that galaxies may have played a major role in this process (Yan & Windhorst 2004; Stiavelli et al. 2004). We take $L^*_{z=3}$ to denote the characteristic luminosity of galaxies at $z = 3$ (Steidel et al. 1999). AB magnitudes are used throughout. We assume $(\Omega_M, \Omega_\Lambda, h) = (0.3, 0.7, 0.7)$ (Bennett et al. 2003).

2. OBSERVATIONS

2.1. *NICMOS Parallels to the UDF*

The two NICMOS parallels to the UDF (taken during the first and second epochs of observations with the Advanced Camera for Surveys [ACS]) make up our primary data set. Each parallel consists of ~160 orbits of data, split between two pointings that overlap by ~25% of a NIC3 pointing (~3.0×10^5 s taken at the first and ~8.6×10^4 s at the second). The observing time at each position was split nearly equally between J_{110} and H_{160} observations. While reductions of these fields are available through STScI, we used the procedures described in Thompson et al. (2005) to perform our own reduction. The deeper of the two pointings making up each parallel had approximate 5 σ depths of 28.6 and 28.5 (0.″6 aperture) in J_{110} and H_{160}, respectively. The shallower pointings were some ~0.6 mag less deep. Our reductions were drizzled onto a 0.″09 pixel scale, with approximate point-spread functions (PSFs) of 0.″32 and 0.″34 FWHM in J_{110} and in H_{160}. For optical coverage on these fields, the V_{606} and z_{850} images from GEMS (Rix et al. 2004; images 25, 42, and 49) were used (Blakeslee et al. 2003).

2.2. *Shallower NICMOS Fields*

To add area at brighter magnitudes, we included a number of other fields with deep $J_{110} + H_{160}$ imaging in our J_{110}-dropout search.

[1] Based on observations made with the NASA/ESA *Hubble Space Telescope*, which is operated by the Association of Universities for Research in Astronomy, Inc., under NASA contract NAS 5-26555.

[2] Department of Astronomy and Astrophysics, University of California, Santa Cruz, 1156 High Street, Santa Cruz, CA 95064.

[3] Steward Observatory, University of Arizona, 933 North Cherry Avenue, Tucson, AZ 85721.

[4] Sterrewacht Leiden, Postbus 9513, NL-2300 RA Leiden, Netherlands.

TABLE 1

J_{110}-DROPOUT SEARCH FIELDS

FIELD	AREA (arcmin^2)	5 σ LIMIT	
		J_{110}	H_{160}
HDF-N Thompson	0.8	27.8	28.1
HDF-N Dickinson	5.2	27.2	27.0
HDF-S NICMOS Parallel	0.8	28.2	28.2
UDF NICMOS Parallel 1	1.3	28.6	28.5
UDF NICMOS Parallel 2	1.3	28.6	28.5
UDF Thompson	5.5	27.7	27.5

A list of these fields is provided in Table 1, together with their approximate 5 σ limiting magnitudes (0.″6 aperture) and selection areas. Other multiwavelength data for these fields include deep *UBVI* coverage for the HDF-N (Williams et al. 1996), ultradeep ACS *BViz* coverage for the UDF (S. V. W. Beckwith et al. 2005, in preparation), NICMOS K_{222} coverage of the HDF-South NICMOS parallel (Williams et al. 2000), and deep IRAC data in the 3.6 μm and 4.5 μm channels for the North and South GOODS fields (M. Dickinson et al. 2005, in preparation).

3. ANALYSIS

SExtractor (Bertin & Arnouts 1996) was used for object detection and photometry. Detection was performed using an aggressive 2 σ detection threshold on the H_{160} images. Our catalogs were then cleaned of contamination from more extended background artifacts by requiring objects to be 5 σ detections in a 0.″5 aperture. We used scaled aperture magnitudes (MAG_AUTO; Kron 1980) for our H_{160} total magnitudes. Colors were also measured with scaled apertures, but with a much smaller Kron factor to maximize the signal-to-noise ratio (S/N). For images with different PSFs, colors were only measured after the higher resolution image had been degraded to match the broader PSF and only in a circular aperture that was at least 2 times the FWHM of the broader PSF (see Bouwens et al. 2003, 2005 [hereafter B05] for more details).

3.1. J_{110}-*Dropout Selection*

Our principal selection criterion was a $(J_{110}-H_{160})_{AB} > 1.8$ color cut, where the flux in J_{110} was replaced by its 1 σ upper limit in cases of a nondetection. This criterion was chosen to minimize contamination from all objects except $z \sim 2$–5 evolved galaxies (Fig. 1). In addition, objects were required to be nondetections (<2 σ) in all optical bands as a result of absorption from the intergalactic medium and to be blue ($\lesssim$1 mag) in all $H_{160}-K$ and $H_{160}-$IRAC colors, since only a small fraction ($\lesssim$2%) of star-forming galaxies have sufficiently red UV continuum slopes β ($\gtrsim$0.5) to produce these colors (Adelberger & Steidel 2000; Schiminovich et al. 2005).

Applying our $(J_{110}-H_{160})_{AB} > 1.8$ color cut to object catalogs from both our primary and shallow search fields, 11 objects were found (Table 2). Of these, six were readily detected (>2 σ) in the bluer optical bands. Two had very red $H_{160}-K$ colors ($\sim$1.5) and so also appear to be low-redshift interlopers. This was a little uncertain for one of the two (HDFSPAR 48278437) because of the marginal nature of its K_{222}-band detection, but IRAC imaging should clarify this issue. The final three sources (shown in Fig. 2 with two red objects from our selection) could not be excluded by either criterion, though this may be largely due to the fact that they were in the UDF parallel fields. The optical imaging in these fields is not particularly deep, nor are there any deep *Spitzer* or *K*-band data to measure colors longward of the break.

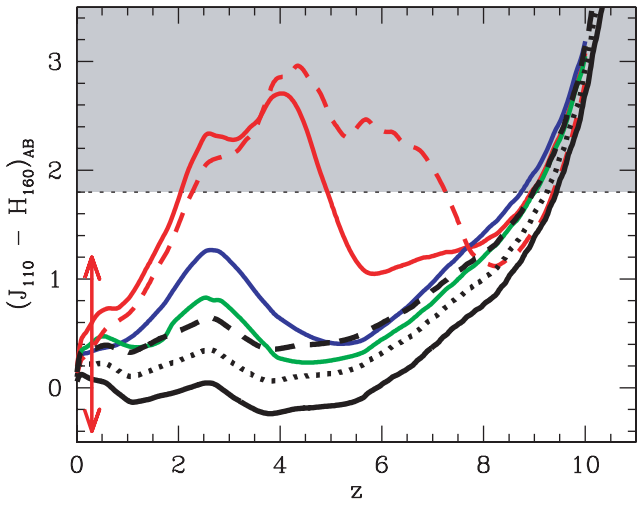

FIG. 1.—$(J_{110}-H_{160})_{AB}$ color vs. redshift for a number of different SEDs. Shown are the Coleman et al. (1980) elliptical, Sbc, and Scd templates (*solid red, blue, and green lines, respectively*), and different reddenings [$E(B-V)$ = 0.0, 0.15, 0.3] applied to a 10^8 yr burst (*black solid, dotted, and dashed lines, respectively*). Extremely red objects (EROs) such as those found in recent IRAC selections (e.g., Yan et al. 2004) have very similar colors (in the infrared) to 2.5 Gyr bursts and are included here as the dashed red line. The arrows near $z \sim 0$ denote the range of colors expected for low-mass stars (Knapp et al. 2004). Our $(J_{110}-H_{160})_{AB} > 1.8$ J_{110}-dropout criterion is shown as a dotted horizontal line and provides a good balance between minimal contamination (selecting evolved SEDs at intermediate redshifts, $z \sim 2$–5) and selecting objects at $z \approx 10$.

3.2. *Low-Redshift Contamination*

To help determine whether the three potential $z \approx 10$ candidates were low-redshift interlopers, we made simple estimates of the contamination from different types of sources. The only known stellar sources red enough to match these objects are extreme carbon stars or Mira variables (Whitelock et al. 1995), but contamination from such sources seems unlikely because of both their rarity and high intrinsic luminosities, which would put them well outside the Galaxy (Dickinson et al. 2000). Contamination from redder, evolved galaxies is difficult to estimate given the large uncertainties on the shape of the luminosity function (LF) of these galaxies at $z \sim 2$–3. Here we ignore these complications and simply scatter the colors of a brighter set of galaxies ($H_{160,AB} \sim 24$–26) from our fields to fainter magnitudes.

TABLE 2

RED OBJECTS $[(J_{110}-H_{160})_{AB} > 1.8]$ IN OUR SEARCH FIELDS

Object ID	R.A. (J2000)	Decl. (J2000)	H_{160}	$J-H$	$V-H$	$z-H$	$H-K$	$H-m_{3.6\,\mu m}$	r_{hl} (arcsec)
UDFNICPAR1 01191115	03 33 01.23	−27 41 11.5	27.0 ± 0.1	1.8	0.9	> −0.2	...	...	0.24
UDFNICPAR1 04151142	03 33 04.18	−27 41 14.1	28.2 ± 0.2	1.8	>0.0	> −1.3	...	...	0.18
UDFNICPAR1 05761077	03 33 05.80	−27 41 07.6	27.8 ± 0.2	>2.0	>0.3	> −1.0	...	...	0.21
UDFNICPAR2 07352493	03 33 07.35	−27 52 49.3	27.9 ± 0.2	1.8	0.6	> −0.7	...	...	0.14

NOTES.—Units of right ascension are hours, minutes, and seconds, and units of declination are degrees, arcminutes, and arcseconds. Magnitudes are on the AB system. All limits are 2 σ except the limits on the $J_{110}-H_{160}$ color, which are only 1 σ. Total magnitudes and colors are derived in Kron apertures of different sizes (B05). Object IDs are the last four significant figures given in this table for the right ascension and declination. Table 2 is published in its entirety in the electronic edition of the *Astrophysical Journal*. A portion is shown here for guidance regarding its form and content.

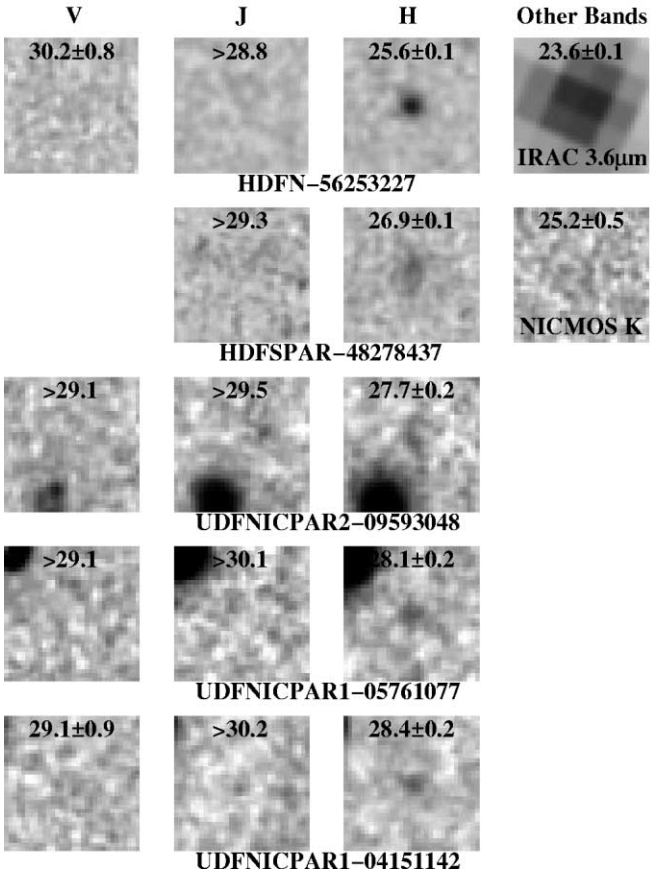

FIG. 2.—Postage-stamp images (J_{110}, H_{160} bands) of five objects that met our $(J_{110}-H_{160})_{AB} > 1.8$ selection. The leftmost and rightmost columns show images in a bluer band (V_{606}) and redder bands (the IRAC 3.6 μm channel for HDFN 56253227 and NICMOS K_{222} for HDFSPAR 48278437), respectively. The overlaid magnitudes (and 1 σ upper limits) were measured within a 0.″6 diameter aperture. The object in the top row (HDFN 56253227) is the well-known Dickinson et al. (2000) J_{110}-dropout. Its extremely red colors $[(H_{160}-K)_{AB} = 1.5$ and $(H_{160}-\mathrm{IRAC}_{3.6\,\mu m})_{AB} = 2]$ suggest that it is at low redshift ($z \sim 2$–3). The second object (HDFSPAR 48278437) was similarly excluded from our list of $z \approx 10$ candidates because of its marginal detection ($\approx 2\,\sigma$) in the NICMOS K_{222} band and $(H_{160}-K_{220})_{AB}$ color of 1.5. The final three objects could be at $z \approx 10$ but await limits at longer wavelengths (from *Spitzer*) and good optical data to exclude the possibility that they are highly reddened or evolved galaxies. UDFNICPAR2 09593048 and UDFNICPAR1 04151142 appear to be just detected in J_{110} at the 1 σ level, so this may indicate they are low-redshift interlopers. The final object (UDFNICPAR1 04151142) is just marginally resolved, but the only stellar sources red enough to match its colors would appear to be too high in luminosity (§ 3.2). Each image is 2.″9 × 2.″9 in size.

Performing these experiments on the faint-source population from the deep parallels, we estimate around one to three such contaminants. This seems consistent with, albeit a little less than, the roughly three sources obtained. A stack of the V_{606} and J_{110} exposures for all three sources showed detections of 0.8 σ and 1.2 σ, respectively, again suggesting some contamination.

3.3. *Expected Numbers/Incompleteness*

Having found at most three possible $z \approx 10$ sources over our entire 14.7 arcmin^{-2} search area, it is interesting to ask how many we might have expected assuming no evolution from lower redshift. Two different redshift samples are considered as baselines: (1) a $z \sim 3.8$ *B*-dropout sample from GOODS (B05), and (2) a $z \sim 6$ *i*-dropout sample from the UDF (R. J. Bouwens et al. 2005, in preparation). As in other recent work (Bouwens et al. 2004a, 2004b, 2004c), we project this sample to higher redshift (over the range $z \sim 7$–13; see Fig. 3) using our well-established cloning machinery (Bouwens et al. 1998a, 1998b, 2003; B05), accounting for pixel

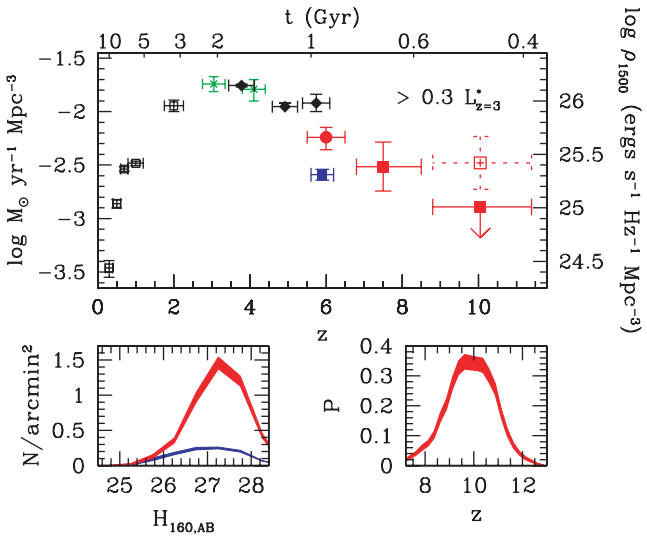

FIG. 3.—*Top*: Cosmic SFR density vs. redshift with no extinction correction. The SFR density (integrated down to $0.3L^*_{z=3}$, the limit of our $z \sim 10$ search) was calculated from the luminosity density in the rest-frame UV continuum (~1500 Å; *right axis*) using canonical assumptions (e.g., Madau et al. 1998) and a Salpeter IMF. The open red square at $z \sim 10$ shows our result if the three objects from this study prove to be at $z \approx 10$, while the downward arrow shows our 1 σ limits if none are. Also included are estimates by Schiminovich et al. (2005; *open black squares*), Steidel et al. (1999; *green crosses*), Giavalisco et al. (2004; *black diamonds*), Bunker et al. (2004; *blue square*), Bouwens et al. (2004c; *filled red square*), and R. J. Bouwens et al. (2005, in preparation; *red circle*). Consistent with past practice, the error bars reflect Poisson uncertainties. Large-scale structure (cosmic variance) would add an estimated ±20% for many of the lower redshift points (see, e.g., Somerville et al. 2004), ±50% for the $z \sim 7.5$ point, and ±19% for the $z \sim 10$ point. *Bottom left*: Surface density of J_{110}-dropouts predicted from a $(1+z)^{-1}$ size scaling of a $z \sim 3.8$ *B*-dropout sample from GOODS (B05) at the depths of the NICMOS parallels to the UDF (*red*). The blue region shows the equivalent surface density for all our search fields. The drop in the predicted counts at fainter magnitudes arises from incompleteness. *Bottom right*: Redshift distribution for objects satisfying our J_{110}-dropout criterion in the above simulations (after distributing our "cloned" objects over the interval $z \sim 7$–13 in proportion to the cosmological volume element). The primary conclusion to be drawn from these results is that there is a significant deficit of bright objects at $z \gtrsim 6$ relative to that present at $z \sim 3$–4.

morphologies, the relationship between distance and angular size, NICMOS PSFs, *k*-corrections, and object-by-object volume densities. Transformed objects are added to the present NICMOS data, and the selection procedure is repeated. Direct use of the data appears to be the best way of accounting for the substantial variations in S/N that occur across NICMOS mosaics while including possible blending with foreground galaxies. Simulations were run over ~30 times the area of the fields. Assuming no evolution in size, 5.7 and 4.1 objects are expected in total (over the six fields) for our $z \sim 3.8$ *B*- and $z \sim 6$ *i*-dropout samples, respectively. If we account for the increase in surface brightness expected from the $\sim(1+z)^{-1}$ size scaling observed at $2 < z < 6$ (Bouwens et al. 2004a, 2004b; Ferguson et al. 2004), the expectations increase to 15.6 and 4.8, respectively. Steeper scalings [i.e., $(1+z)^{-2}$] yield 21.2 and 6.3 J_{110}-dropouts, respectively, while use of a bluer UV continuum slope β (e.g., $\beta \sim -2.4$) resulted in 16.2 and 4.0, respectively [assuming a $(1+z)^{-1}$ size scaling]. We note that the two NICMOS parallels to the UDF account for ~73% of the expected numbers (and are therefore our primary constraints), though each of the six fields contributes at least a few percent. We take the $(1+z)^{-1}$ scaling estimates, 15.6 from $z \sim 3.8$ and 4.8 from $z \sim 6$, as the most likely expected values.

3.4. *Previous Work*

One previous study of $z \gtrsim 8$ candidates was carried out by Yahata et al. (2000) on the 0.8 arcmin^2 NIC3 parallel to the

HDF-South featured here. In that paper, eight $z \gtrsim 10$ candidates were reported (five of which were selected in the H_{160} band) based on nine-band (*UBVRIJHK* + STIS) photometric redshifts. What became of these five candidates here? Looking through our catalogs for this field, we found that one (SB-NI 0915-0620) had $J_{110}-H_{160}$ colors (~0.4) clearly inconsistent with a high-redshift identification. The other four appeared to be too faint ($H_{160,AB} \gtrsim 27.5$) to set strong lower limits on the $(J_{110}-H_{160})_{AB}$ colors and thus make robust statements about their redshifts.

4. IMPLICATIONS

We have carried out a search for $z \approx 10$ *J*-dropouts and found at most three possible candidates. Since 15.6 ± 3.9 and 4.8 ± 2.2 candidates are expected (Poisson errors) based on a $(1+z)^{-1}$ scaling of $z \sim 3.8$ and $z \sim 6$ samples, this suggests that there has been appreciable evolution at the bright end of the luminosity function. Since an $L^*_{z=3}$ galaxy at $z \sim 10$ has an $H_{160,AB}$ magnitude of 26.7, our search ($H_{160,AB} \lesssim 28$) tells us something about the galaxy luminosities brightward of $0.3L^*_{z=3}$. For simple Poisson statistics and assuming that all three sources are at $z \approx 10$, the current findings are inconsistent with no evolution at the 99.98% and 71% confidence levels, respectively (equivalent to 3.8 σ and 1 σ).

Of course, cosmic variance is bound to be important for fields of this size. Assuming a selection window of width $\Delta z = 2.5$, a ΛCDM power spectrum, and a bias of 7—which corresponds to the rough volume density of sources $\sim 10^{-4}$ Mpc^{-3} explored by this probe (Mo & White 1996)—we calculate ~27% rms variations from field to field for single 0.8 arcmin^2 NIC3 pointings (using a pencil-beam window function). Since our deepest two fields provide the primary constraints and they are essentially independent, the total number of *J*-dropouts found here is expected to vary by ~19% rms relative to the cosmic average. Thus, we expect ~16 ± 5 and ~5 ± 2 dropouts, respectively, for simple projections of our lower redshift samples, and so the present findings are inconsistent with no evolution at the 99.9% and 68% confidence levels, respectively (equivalent to 3.3 σ and 1.0 σ).

It is conventional to cast such findings in terms of the rest-frame continuum UV (~1500 Å) luminosity density. We first estimate the luminosity density under the assumption that the three candidates are at $z \approx 10$. The result is $\rho_{UV}(z \sim 10)/\rho_{UV}(z \sim 3.8) = 0.19^{+0.13}_{-0.09}$ (3/15.6 for Poisson statistics) or $\rho_{UV}(z \sim 10)/\rho_{UV}(z \sim 3.8) = 0.19^{+0.15}_{-0.10}$ (including cosmic variance). Taking the value of the luminosity density at $z \sim 3.8$ (Giavalisco et al. 2004) integrated down to $0.3L^*_{z=3}$, we find a UV luminosity density $\rho_{UV}(z \sim 10) = 2.5^{+1.7}_{-1.2} \times 10^{25}$ ergs s^{-1} Hz^{-1} (Poisson statistics) or $\rho_{UV}(z \sim 10) = 2.5^{+2.0}_{-1.3} \times 10^{25}$ ergs s^{-1} Hz^{-1} (with cosmic variance). However, it is plausible that none of these candidates are at $z \approx 10$. The expected high contamination level, combined with the now well established changes in the LF between $z \sim 6$–7 and $z \sim 3$, suggests that it is more likely that these sources are low-redshift objects. Assuming that none are at $z \approx 10$, the 1 σ upper limit is $\rho_{UV}(z \sim 10)/\rho_{UV}(z \sim 3.8) < 0.07$ (both for simple Poisson statistics and including cosmic variance). In terms of the luminosity density, this limit is $\rho_{UV}(z \sim 10) < 0.9 \times 10^{25}$ ergs s^{-1} Hz^{-1}. Adopting a Salpeter initial mass function (IMF) and using canonical relations to convert this into a star formation rate (SFR) density (Madau et al. 1998), we can plot the present determination (integrated down to $0.3L^*_{z=3}$) against previous determinations at lower redshift (Fig. 3). The observations now more clearly than before allow us to trace the number of UV-bright systems over the interval $0 < z < 10$. The space density of high-luminosity systems seems to peak at $z \sim 2$–4 and decline fairly rapidly to higher and lower redshifts.

As we conclude, it is somewhat sobering to realize that ~800 orbits of deep NICMOS imaging went into this search and only three possible $z \approx 10$ candidates were found (all of which may be at low redshift), showing how difficult it is to map out the formation of galaxies at these early times with current technology. It is exciting nevertheless to realize that in the future these surveys will be executed much more efficiently. For example, surpassing the current NICMOS data set would require just ~23 orbits with *HST* WFC3 and ~1000–2000 s with *JWST*.

We are grateful to S. Beckwith and the entire STScI science team for their foresight in taking deep NICMOS parallels to the UDF, M. Dickinson and STScI for making their NICMOS reductions available in electronic form, D. Eisenstein, B. Mobasher, and E. Scannapieco for valuable discussions, H. Yan for an electronic copy of a 2.5 Gyr ERO SED, and our referee for valuable comments that substantially improved this manuscript. This research was supported under NASA grants GO-09803.05-A and NAG 5-7697.

REFERENCES

Adelberger, K. L., & Steidel, C. C. 2000, ApJ, 544, 218
Bennett, C. L., et al. 2003, ApJ, 583, 1
Bertin, E., & Arnouts, S. 1996, A&AS, 117, 393
Blakeslee, J. P., Anderson, K. R., Meurer, G. R., Benítez, N., & Magee, D. 2003, in ASP Conf. Ser. 295, Astronomical Data Analysis Software and Systems XII, ed. H. E. Payne, R. I. Jedrzejewski, & R. N. Hook (San Francisco: ASP), 257
Bouwens, R., Broadhurst, T., & Illingworth, G. 2003, ApJ, 593, 640
Bouwens, R., Broadhurst, T., & Silk, J. 1998a, ApJ, 506, 557
———. 1998b, ApJ, 506, 579
Bouwens, R. J., Broadhurst, T. J., Illingworth, G. D., Meurer, G. R., Blakeslee, J. P., Franx, M., & Ford, H. C. 2005, ApJ, submitted (B05)
Bouwens, R. J., Illingworth, G. D., Blakeslee, J. P., Broadhurst, T. J., & Franx, M. 2004a, ApJ, 611, L1
Bouwens, R. J., et al. 2004b, ApJ, 606, L25
———. 2004c, ApJ, 616, L79
Bunker, A. J., Stanway, E. R., Ellis, R. S., & McMahon, R. G. 2004, MNRAS, 355, 374
Coleman, G. D., Wu, C.-C., & Weedman, D. W. 1980, ApJS, 43, 393
Dickinson, M. 1999, in AIP Conf. Proc. 470, After the Dark Ages: When Galaxies Were Young, ed. S. S. Holt & E. P. Smith (Woodbury, NY: AIP), 122
Dickinson, M., et al. 2000, ApJ, 531, 624
Ferguson, H. C., et al. 2004, ApJ, 600, L107
Giavalisco, M., et al. 2004, ApJ, 600, L103
Knapp, G. R., et al. 2004, AJ, 127, 3553
Kogut, A., et al. 2003, ApJS, 148, 161
Kron, R. G. 1980, ApJS, 43, 305
Madau, P., Pozzetti, L., & Dickinson, M. 1998, ApJ, 498, 106
Mo, H. J., & White, S. D. M. 1996, MNRAS, 282, 347
Rix, H.-W., et al. 2004, ApJS, 152, 163
Schiminovich, D., et al. 2005, ApJ, 619, L47
Somerville, R. S., Lee, K., Ferguson, H. C., Gardner, J. P., Moustakas, L. A., & Giavalisco, M. 2004, ApJ, 600, L171
Steidel, C. C., Adelberger, K. L., Giavalisco, M., Dickinson, M., & Pettini, M. 1999, ApJ, 519, 1
Stiavelli, M., Fall, S. M., & Panagia, N. 2004, ApJ, 610, L1
Thompson, R. I., Storrie-Lombardi, L. J., Weymann, R. J., Rieke, M. J., Schneider, G., Stobie, E., & Lytle, D. 1999, AJ, 117, 17
Thompson, R. I., et al. 2005, AJ, in press (astro-ph/0503504)
Whitelock, P., Menzies, J., Feast, M., Catchpole, R., Marang, F., & Carter, B. 1995, MNRAS, 276, 219
Williams, R. E., et al. 1996, AJ, 112, 1335
———. 2000, AJ, 120, 2735
Yahata, N., Lanzetta, K. M., Chen, H.-W., Fernández-Soto, A., Pascarelle, S. M., Yahil, A., & Puetter, R. C. 2000, ApJ, 538, 493
Yan, H., & Windhorst, R. A. 2004, ApJ, 612, L93
Yan, H., et al. 2004, ApJ, 616, 63